Title: Multi-generational silencing dynamics control cell aging

Authors: Yang Li[1]†, Meng Jin[3]†, Richard O'Laughlin[2]†, Lev S. Tsimring[3], Lorraine Pillus[1,4], Jeff Hasty[1,2,3]* and Nan Hao[1,3]*

Affiliations:

[1]Section of Molecular Biology, Division of Biological Sciences, University of California San Diego, La Jolla, CA 92093, USA.

[2]Department of Bioengineering, University of California San Diego, La Jolla, CA 92093, USA.

[3]BioCircuits Institute, University of California San Diego, La Jolla, CA 92093, USA.

[4]UCSD Moores Cancer Center, University of California San Diego, La Jolla, CA 92093, USA.

*Correspondence to: Jeff Hasty, jhasty@eng.ucsd.edu; Nan Hao, nhao@ucsd.edu

†These authors contributed equally to this work.

Cellular aging plays an important role in many diseases [1], such as cancers [2], metabolic syndromes [3] and neurodegenerative disorders [4]. There has been steady progress in identifying age-related factors such as reactive oxygen species and genomic instability [5], yet an emerging challenge is to reconcile the mechanistic contributions of these factors with the fact that genetically identical cells can age at significantly different rates. Single-cell analyses to unravel the interplay of aging dynamics and variability hold the promise to answer that challenge [6-8]. We have used novel microfluidic technologies to track the replicative aging of single yeast cells, revealing that cells show sporadic waves of silencing loss in the heterochromatic ribosomal DNA (rDNA) during early phases of aging, followed by sustained loss of silencing preceding cell death. Isogenic cells have different lengths of the early intermittent silencing phase that largely determine their final lifespans. Combining computational modeling and experimental approaches, we found that the intermittent silencing dynamics is important for longevity and is dependent on the conserved Sir2 deacetylase, whereas either sustained silencing or sustained loss of silencing shortens lifespan. These findings reveal a new dynamics-based control of cell aging that could guide the design of temporally controlled nutriceutical strategies to extend lifespan.

Main Text:

Replicative aging of yeast is measured as the number of daughter cells produced before the death of a mother cell [9]. The conventional method for studying yeast aging requires laborious manual separation of daughter cells from mother cells after each division and does not allow tracking of molecular processes over multiple generations during aging [5]. Recent advances in microfluidics technology have automated cell separation and enabled continuous single-cell

measurements during aging [10-16]. Building upon these efforts, we developed a new microfluidic aging device. The device traps mother cells at the bottom of finger-shaped chambers, allowing them to bud continuously, while daughter cells are removed via a waste port. Each chamber also has a small opening at the bottom, allowing daughter removal when mother cells switch budding direction (Fig. 1a, b and Supplementary Movie 1). The long trapping chambers allow tracking of each daughter cell during its first several divisions, useful for monitoring age-related daughter morphologies. Furthermore, the device can deliver precise environmental waveforms to culture chambers. In validating the device, we confirmed that the majority of loaded cells are exponentially-growing newborn or young cells and the Replicative Lifespans (RLS) of wild-type (WT) cells in the device are comparable to those from classical microdissection [17] (Supplementary Fig. 1a, b).

Genome instability has been considered a significant causal factor of cell aging [18,19]. A major contributor to the maintenance of genome stability is chromatin silencing, which causes a locally inaccessible heterochromatin structure that suppresses transcription, recombination and DNA damage. The heterochromatic regions in yeast include the silent mating-type loci, rDNA and subtelomeric regions [20]. Among them, the rDNA region on chromosome XII consists of 100~200 tandem repeats and is a particularly fragile genomic site, the stability of which closely connects to the RLS [21-23]. How chromatin silencing changes during aging remains largely unknown. To measure silencing in single aging cells, we constructed a strain with a fluorescent reporter gene under the control of a constitutive *TDH3* promoter at a non-transcribed spacer region (NTS1) of rDNA. Because expression of the reporter gene is suppressed by silencing, decreased fluorescence indicates enhanced silencing, whereas increased fluorescence indicates reduced silencing [24,25] (Fig. 1c). We observed that cells with the rDNA reporter gene exhibit

weak fluorescence; in contrast, cells carrying the same reporter at the *URA3* locus, which is not subject to silencing, show very high fluorescence. In addition, deletion of *SIR2*, which is required for rDNA silencing [20], yields significantly increased reporter expression at the rDNA, but not at *URA3* (Supplementary Fig. 1c).

Using the microfluidic device and the reporter, we tracked the dynamics of rDNA silencing throughout the entire lifespans of individual cells (Fig. 1d; Fig. 2) We found intermittent fluorescence increases in most cells, indicating sporadic silencing loss during aging. In addition, about half of the cells exhibited a sustained and dramatic increase in fluorescence at the later stage of their lifespans, indicating sustained loss of silencing in aged cells. Interestingly, all of these aged cells continuously produced daughter cells with a characteristic elongated morphology until death (Fig. 2a). In contrast, the other half of the cells did not show sustained silencing loss or elongated daughters before death (Fig. 2b). Instead, they produced small round daughter cells with dramatically increased cell cycle length before death and had a shorter average lifespan (with a mean RLS of 18, compared to 24). These two distinct types of age-associated phenotypic changes suggest different causes of aging in isogenic cells [10-12]. Our results revealed that sustained rDNA silencing loss, which can lead to genome instability [20], is specifically associated with the aging phenotype characterized by elongated daughters. In support of this, young mother cells can also sporadically produce a few elongated daughters, the occurrence of which correlates with the transient silencing loss during the early phase of their lifespans (Fig. 2c; Supplementary Fig. 2).

To exclude the possibility that the observed fluorescence patterns are caused by age-associated global effects on gene expression [26], we simultaneously monitored two distinguishable fluorescent reporters inserted at the rDNA and at *URA3*. Whereas the rDNA reporter showed

early sporadic and late sustained induction of fluorescence, the reporter at *URA3* exhibited relatively constant fluorescence during aging (Supplementary Fig. 3a). To confirm that the observed silencing dynamics are not specific to the NTS1 region, we measured the reporter response at another non-transcribed spacer region of rDNA (NTS2) and observed similar dynamic patterns as those found at NTS1 (Supplementary Fig. 3b). Together, these results validate the reporter responses during aging. Finally, we observed very rare events of recombination or extrachromosomal rDNA circles of the reporter gene, which can be easily distinguished from silencing loss in single-cell time traces (Supplementary Fig. 3c). We have excluded those cells from the analysis.

To evaluate how dynamic patterns of chromatin silencing influence cell aging, we quantitatively analyzed the time traces of silencing loss in individual cells producing elongated daughters before death. With very diverse lifespans ranging from 9 to 48 generations, all of the cells show sustained silencing loss toward later stages of aging. Most cells also exhibit early sporadic waves of silencing loss, each of which spans multiple cell divisions (Fig. 3a). This unprecedented long-wavelength dynamics is distinct from most previously characterized molecular pulses, which are on timescales faster than or close to a cell cycle [8]. We further dissected each single-cell time trace into two phases: an early phase with sporadic silencing loss and a late phase with sustained silencing loss (Fig 3b, "Intermittent Phase" and "Sustained Phase"). The length of Intermittent Phase (or the number of silencing waves) is highly variable among cells (Coefficient of Variation – CV: 0.63; Supplementary Fig. 4a) and correlates closely with final lifespan, suggesting that the longevity of a cell is largely determined by the time it stays in this phase (Fig. 3c, left). Long-lived cells generally have a longer Intermittent Phase and produce more silencing waves than short-lived cells (Fig. 3a; Supplementary Fig. 4b). In

contrast, the length of Sustained Phase is more uniform among cells (CV: 0.29; Supplementary Fig. 4a) and shows little relationship with lifespan, suggesting that sustained silencing loss defines cell death within a relatively constant period of time (Fig. 3c, right). We further quantified the rise time of each fluorescence increase in single aging cells (the duration of silencing loss; Fig. 3b, t1 and t2) and found a significant difference between the durations of early sporadic and later sustained silencing loss: a sporadic silencing loss on average lasts for ~ 300 minutes, whereas sustained silencing loss lasts for ~ 1200 minutes until death (Fig. 3d). Moreover, sporadic silencing loss does not contribute additively onto sustained silencing loss to inducing cell death (Supplementary Fig. 4c). Together, our analyses reveal that cells undergo spontaneous silencing loss during aging. The early phase of aging features a reversible process, in which cells can effectively re-establish silencing and produce non-detrimental short waves of silencing loss. The late phase is irreversible: aged cells cannot re-establish silencing [27], resulting in sustained silencing loss and death. Individual cells might have different intrinsic capacities to maintain the reversible phase and thereby the ultimate lifespan.

To provide a quantitative framework for understanding aging dynamics, we developed a simple phenomenological model. The model postulates that an aging cell can be in one of two states: state 0 is the silenced state in which it produces normal daughters, and state 1 is the silencing loss state with elongated daughters (Fig. 4a). The transitions between the states are characterized by probabilities p_{01} and p_{10} that depend on the cell age (Fig. 4b). We also assume that in the silencing loss state (state 1), a damage factor D accumulates over generations and the probability of cell death increases with D according to a Poisson cumulative distribution function (Fig. 4c). In the silenced state (state 0), D is set to zero. We simulated this model stochastically and generated 100 cell trajectories (Fig. 4d) that qualitatively and quantitatively

reproduce the data in Fig. 2a. To predict how silencing dynamics influence aging, we further simulated the effects of an induced silencing loss. Whereas a short pulse of silencing loss does not affect lifespan, a sustained silencing loss dramatically shortens lifespan (Fig. 4e). To test these predictions, we set out to modify silencing dynamics using genetic or chemical perturbations.

Chromatin silencing at the rDNA is primarily mediated by the lysine deacetylase Sir2, encoded by the best-studied longevity gene to date, which is conserved from bacteria to humans [20]. To examine the role of Sir2 in regulating silencing dynamics, we monitored the aging process of *sir2Δ* cells. We observed that *sir2*Δ cells do not exhibit sporadic silencing loss; instead, most cells show sustained silencing loss throughout their lifespans (Fig. 5a), indicating that the intermittent silencing dynamics during WT aging is dependent on Sir2-mediated silencing re-establishment. Furthermore, in *sir2*Δ cells, sustained silencing loss leads to cell death within a relatively uniform time frame, consistent with the model prediction (Fig. 4e, left) and strikingly resembling the Sustained Phase in WT cells (Fig. 5a, red dashed line). These results suggest that Sir2 promotes longevity by generating intermittent silencing dynamics and delaying entry into the Sustained Phase.

To further test predictions of the model and examine the causative roles of silencing dynamics on aging, we exposed cells to nicotinamide (NAM), an inhibitor of Sir2 [28], to chemically disrupt silencing with physiologically relevant durations. In response to a 1000-minute NAM input mimicking Sustained Phase, the majority of cells cannot recover from silencing loss and die within a similar time frame to sustained silencing loss in *sir2* mutant or WT cells (Fig. 5b). The cells show an elevated DNA damage response, as reported by the induction of *RNR3* [29,30] (Fig. 5b, inset), and have a significantly shortened lifespan (mean RLS:

12), comparable to that of *sir2* mutants. In contrast, in response to a 240-minute NAM input, mimicking the sporadic silencing loss, most cells exhibit a synchronized silencing loss followed by effective silencing re-establishment upon the removal of NAM (Fig. 5c). This short-term silencing loss does not induce the DNA damage response (Fig. 5c, inset) and does not affect lifespan, in accord with the sporadic silencing loss in Intermittent Phase of naturally aging cells. These results validate the model's predictions and confirm that a prolonged duration of silencing loss triggers an irreversible process sufficient to induce cell death, whereas short-term silencing loss is fully reversible and does not promote aging or death.

Finally, we considered the role of intermittent dynamics of silencing, as opposed to continuous chromatin silencing. To this end, we used nicotinic acid (NA), an activator of Sir2 [31], to prevent sporadic silencing loss in aging cells. As shown in Fig. 5d, most cells show continuous silencing with fewer sporadic losses of silencing. Surprisingly, however, sustained chromatin silencing, similar to sustained silencing loss, also results in significantly shortened lifespan (mean RLS: 11). These effects of NA are mediated through Sir2 (Supplementary Fig. 5) and hence might be caused by a constant Sir2-mediated repression of pro-longevity factors.

Taken together, our results suggest the intriguing possibility that chromatin silencing may be a double-edged sword with both anti-aging and pro-aging functions, probably depending on target genomic regions. Whereas sustained rDNA silencing loss increases heterochromatin instability, sustained chromatin silencing may suppress genes that benefit longevity; either state would accelerate cell aging and death. The intermittent silencing dynamics driven by Sir2 allow the cell to periodically alternate between the two states, maintaining a time-based balance important for longevity. Our findings thus highlight the significant role of silencing dynamics in

cellular aging, which deserves careful consideration when designing nutriceutical schemes to extend lifespan by modulating sirtuins.

References:

1 Kennedy, B. K. *et al.* Geroscience: linking aging to chronic disease. *Cell* **159**, 709-713 (2014).
2 DePinho, R. A. The age of cancer. *Nature* **408**, 248-254 (2000).
3 Morley, J. E. The metabolic syndrome and aging. *J Gerontol A Biol Sci Med Sci* **59**, 139-142 (2004).
4 Lin, M. T. & Beal, M. F. Mitochondrial dysfunction and oxidative stress in neurodegenerative diseases. *Nature* **443**, 787-795 (2006).
5 Steinkraus, K. A., Kaeberlein, M. & Kennedy, B. K. Replicative aging in yeast: the means to the end. *Annu Rev Cell Dev Biol* **24**, 29-54 (2008).
6 Purvis, J. E. & Lahav, G. Encoding and decoding cellular information through signaling dynamics. *Cell* **152**, 945-956 (2013).
7 Behar, M. & Hoffmann, A. Understanding the temporal codes of intra-cellular signals. *Curr Opin Genet Dev* **20**, 684-693 (2010).
8 Levine, J. H., Lin, Y. & Elowitz, M. B. Functional roles of pulsing in genetic circuits. *Science* **342**, 1193-1200 (2013).
9 Mortimer, R. K. & Johnston, J. R. Life span of individual yeast cells. *Nature* **183**, 1751-1752 (1959).
10 Lee, S. S., Avalos Vizcarra, I., Huberts, D. H., Lee, L. P. & Heinemann, M. Whole lifespan microscopic observation of budding yeast aging through a microfluidic dissection platform. *Proc Natl Acad Sci U S A* **109**, 4916-4920 (2012).
11 Xie, Z. *et al.* Molecular phenotyping of aging in single yeast cells using a novel microfluidic device. *Aging Cell* **11**, 599-606 (2012).
12 Jo, M. C., Liu, W., Gu, L., Dang, W. & Qin, L. High-throughput analysis of yeast replicative aging using a microfluidic system. *Proceedings of the National Academy of Sciences of the United States of America* (2015).
13 Liu, P., Young, T. Z. & Acar, M. Yeast Replicator: A High-Throughput Multiplexed Microfluidics Platform for Automated Measurements of Single-Cell Aging. *Cell reports* **13**, 634-644 (2015).
14 Zhang, Y. *et al.* Single cell analysis of yeast replicative aging using a new generation of microfluidic device. *PloS one* **7**, e48275 (2012).
15 Fehrmann, S. *et al.* Aging yeast cells undergo a sharp entry into senescence unrelated to the loss of mitochondrial membrane potential. *Cell reports* **5**, 1589-1599 (2013).
16 Crane, M. M., Clark, I. B., Bakker, E., Smith, S. & Swain, P. S. A microfluidic system for studying ageing and dynamic single-cell responses in budding yeast. *PloS one* **9** (2014).
17 Steffen, K. K., Kennedy, B. K. & Kaeberlein, M. Measuring replicative life span in the budding yeast. *Journal of visualized experiments : JoVE* (2009).
18 Vijg, J. & Suh, Y. Genome instability and aging. *Annu Rev Physiol* **75**, 645-668 (2013).
19 McMurray, M. A. & Gottschling, D. E. Aging and genetic instability in yeast. *Curr Opin Microbiol* **7**, 673-679 (2004).

20 Gartenberg, M. R. & Smith, J. S. The Nuts and Bolts of Transcriptionally Silent Chromatin in Saccharomyces cerevisiae. *Genetics* **203**, 1563-1599 (2016).
21 Saka, K., Ide, S., Ganley, A. R. & Kobayashi, T. Cellular senescence in yeast is regulated by rDNA noncoding transcription. *Curr Biol* **23**, 1794-1798 (2013).
22 Lindstrom, D. L., Leverich, C. K., Henderson, K. A. & Gottschling, D. E. Replicative age induces mitotic recombination in the ribosomal RNA gene cluster of Saccharomyces cerevisiae. *PLoS Genet* **7**, e1002015 (2011).
23 Sinclair, D. A. & Guarente, L. Extrachromosomal rDNA circles--a cause of aging in yeast. *Cell* **91**, 1033-1042 (1997).
24 Xu, E. Y., Zawadzki, K. A. & Broach, J. R. Single-cell observations reveal intermediate transcriptional silencing states. *Mol Cell* **23**, 219-229 (2006).
25 Dodson, A. E. & Rine, J. Heritable capture of heterochromatin dynamics in Saccharomyces cerevisiae. *eLife* **4**, e05007 (2015).
26 Hu, Z. *et al.* Nucleosome loss leads to global transcriptional up-regulation and genomic instability during yeast aging. *Genes Dev* **28**, 396-408 (2014).
27 Dang, W. *et al.* Histone H4 lysine 16 acetylation regulates cellular lifespan. *Nature* **459**, 802-807 (2009).
28 Kato, M. & Lin, S. J. Regulation of NAD+ metabolism, signaling and compartmentalization in the yeast Saccharomyces cerevisiae. *DNA Repair (Amst)* **23**, 49-58 (2014).
29 Elledge, S. J. & Davis, R. W. Two genes differentially regulated in the cell cycle and by DNA-damaging agents encode alternative regulatory subunits of ribonucleotide reductase. *Genes Dev* **4**, 740-751 (1990).
30 Xie, Z. *et al.* Early telomerase inactivation accelerates aging independently of telomere length. *Cell* **160**, 928-939 (2015).
31 Evans, C. *et al.* NAD+ metabolite levels as a function of vitamins and calorie restriction: evidence for different mechanisms of longevity. *BMC Chem Biol* **10**, 2 (2010).

Acknowledgments: We thank Dr. Danesh Moazed (Harvard Medical School) for providing the pDM714 and pDM312 plasmids. We thank Yuan Zhao (Bioinformatics, UCSD) for helping with developing the image analysis code, and Dr. Philbert Tsai (Physics, UCSD) for helping with the super-resolution confocal microscopy. This work was supported by NIH R01 GM111458 (to N.H.), UC Cancer Research Coordinating Committee (to L.P.) and DoD, Air Force Office of Scientific Research, National Defense Science and Engineering Graduate (NDSEG) Fellowship, 32 CFR 168a (to R.O.).

Author Contributions: Y. L. conducted the experimental analysis. M. J. developed the computational model. R. O. developed the microfluidic device. Y. L., M. J., and R. O. performed data analysis. Y. L., M. J., R. O., L.S.T, L.P., J.H. and N.H. conceived the project and wrote the paper.

Methods:

Strains and plasmids construction

Standard methods for the growth, maintenance and transformation of yeast and bacteria for manipulation of DNA were used throughout. The yeast strains used in this study were generated from BY4741 (*MAT a his3Δ1 leu2Δ0 met15Δ0 ura3Δ0*) strain background. Strain and plasmid information is provided in Supplementary Tables 1 and 2.

To make the nuclear reporter for single cells, a *IRFP::KanMX* fragment was PCR amplified and integrated into the C-terminus of *NHP6a* at the native locus by homolog recombination. To make *sir2Δ* mutants, a *CgHIS3*[32] fragment was amplified to replace the *SIR2* open reading frame by homolog recombination. Similarly, the *SGF73* ORF was replaced with *CgHIS3*. The *URA3* ORF is deleted in the BY4741 background. To add a mutated *URA3* gene (*ura3-1*) back to its native locus, a *CgURA3* fragment [32] was amplified and inserted at *URA3*, then *CgURA3* was replaced with a *ura3-1* allele from the W303 strain.

To make the *NTS1* silencing reporter, a *Xho*1-*NTS1*-*Eco*RI fragment from pDM704 [33] was ligated into the pRS306 plasmid vector. A *Eco*RI-P_{TDH3}-*GFP*-*Eag*I fragment contains 680 bp of *TDH3* promoter and *GFP* ORF was made by fusion PCR and then ligated into pRS306 and the plasmid pRS306 with *Xho*1-*NTS1*-*Eco*RI fragment to get plasmids NHB0206 and NHB0200. Plasmids NHB0213 and NHB0214 were constructed in the same way. The *NTS2* fragment for plasmid NHB0214 was derived from plasmid pDM312[33]. Yeast strains with rDNA silencing reporter were generated by transformation with NHB0200 cut with *Hind*III to integrate at *NTS1*, NHB0213 cut with *Hind*III to integrate at *NTS1*, NHB0214 cut with *Sma*I to integrate at *NTS2*, and NHB0206 cut with *Stu*I to integrate at *ura3-1*. All transformations were performed with the lithium acetate method [34], and integration was confirmed by PCR.

Quantification of bud scar numbers

Yeast cells were inoculated into 2 ml of synthetic drop-out (SD) medium and cultured overnight at 30°C. 2 μl of saturated culture was diluted into 20 ml of fresh SD medium and grown at 30°C overnight. To check the age distribution of yeast cells, cultures with different OD600 were sampled and stained with 5 μg/ml WGA conjugates (Alexa Fluor 647 conjugate, Thermo Fisher) for 10 min at 37°C. Cells were washed twice with PBS after incubation then examined with a Leica TCS SP8 Stimulated Emission Depletion (STED) super-resolution microscope using a Cy5.5 channel to visualize the budding scars.

Design and fabrication of the microfluidic device for yeast aging studies

In designing a microfluidic device for studying aging in budding yeast, the viability of the cells, efficiency of cell trapping and robustness of the device were our primary concerns. Multiple designs were built and tested to optimally satisfy these criteria. The robustness of the device is affected by clogging due to excess cells around the traps and at the waste port, which can interfere with mother cell lifespan and retention. Supplying media through ~20 μm tall main channels readily allowed excess cells to be washed away and prevented clogging. Therefore, a critical feature of our device is its two-layer design, making it extremely robust over the course of our 80-hour experiments. This is a unique feature compared to recently published devices that are all single-layer [12,13,16]. The device was optimized for using continuous gravity-driven flow during operation, with the three-inlet design also facilitating media switching experiments. Cell loading efficiencies and final retentions until cell death are approximately 93% and 75% respectively.

To construct the microfluidic device, designs were first drawn in AutoCAD (Autodesk Inc.). Modeling of fluid flow in the device using COMSOL Multiphysics aided in design (COMSOL Inc.). Two chrome quartz glass masks (HTA Photomask), one for each layer of the device, were used to pattern SU-8 negative epoxy photoresist (MicroChem Corp.) onto clean silicon wafers (University Wafer Inc.). SU-8 2005 was used to build the first layer (cell trapping region) and was spun at 3250 rpm while SU-8 2015 was used to build the second layer (main channels), spun at 2000 rpm. These spin parameters yield approximately 4.3 μm and 20 μm tall features for the cell trapping and main channel layers respectively, as measured by a Dektak 150 surface profiler (Veeco Instruments Inc.). The mask for the second layer was aligned to the first layer of the wafer using an EVG620 mask aligner (EV Group Inc.). Once patterning of the SU-8 was complete, the wafer was exposed to 40 μl of trichloro(1H, 1H, 2H, 2H-perfluoro-octyl)silane (Sigma-Aldrich Co.) in a vacuum chamber for 7 minutes. After this poly-dimethylsiloxane (PDMS, Sylgard 184, silicone elastomer kit with base and curing agent, Dow Corning Corp.) molds of the features on the wafer were made, cleaned and bonded to glass coverslips for experiments as described in [35].

Setting up a microfluidics experiment

Each microfluidic device was checked carefully to ensure no dust or broken features before use. Cells were cultured as described above to start experiments at $OD600_{nm}$ of 1.0. For loading, cells were transferred into a 60 ml syringe (Luer-Lok Tip, BD) connected to plastic tubing (TYGON, ID 0.020 IN, OD 0.060 IN, wall 0.020 IN). Before setting up a microfluidics experiment, the device was vacuumed for 20 min. After vacuum, all of the inlets of the device were covered with 0.075% Tween 20 (Sigma-Aldrich Co.) for 5 min. The microfluidic device was placed on the stage of an inverted microscope with a 30°C incubator system. Three media ports were connected to plastic tubing, which connected to 60 ml syringes with fresh SD medium containing 0.04% Tween. The height of all three medium syringes is about 20 inches above the stage. The waste port of the microfluidic device was connected to plastic tubing, which was set to stage height. To load cells, the connected syringe on the middle port was replaced with a syringe filled with yeast culture. The height of the cell-loading syringe is also about 20 inches above the stage. The flow of medium in the device was maintained by gravity and drove cells into traps. Most traps were filled with cells within2-5 minutes, after which cell loading tubing was replaced with supply tubing and syringe as above. Then the height of all medium tubing and the waste tubing were adjusted to make the height difference around 60 inches. Waste medium was collected in a 50 ml tube to measure flow rate, which was about 2.5 ml/day.

For experiments with media switching, left and right medium ports were connected to syringes with fresh SD medium containing 0.04% Tween and the middle medium port was connected to a syringe containing medium with NA or NAM and 0.1 μg/ml Atto 655 cy5 dye (Sigma 93711). The waste port of the microfluidic device was connected to plastic tubing set to a position about 20 inches below the stage. Before cell loading, the heights of syringes need to be calibrated for media switching. Syringes connected to the left and right medium ports were moved to the same height as the microscope stage and the syringe containing NA or NAM was moved to about 33 inches above the stage. To further calibrate the positions, the junction of all three medium channels was imaged under the cy5 channel and the positions of syringes were adjusted to ensure the medium channel was fully filled with the NA or NAM medium. The position of all syringes

were marked and used for NA or NAM during the experiment. To switch from the NA or NAM medium to SD medium, the left and right syringes were moved to about 33 inches above the stage and the middle syringes was moved to the same height as the stage. The positions of all syringes were further calibrated under the cy5 channel to ensure no SD medium went into the cell trapping region and then marked the positions of all syringes for the condition of no NA or NAM in the cell culture chamber. Cell loading was as for experiments without media switching. After cell loading, all syringes were moved to previously marked positions. The flow rate is about 2.5 ml/day.

Time-lapse microscopy

Time-lapse microscopy experiments were performed using a Nikon Ti-E inverted fluorescence microscope with Perfect Focus, coupled with an EMCCD camera (Andor iXon X3 DU897). The light source is a spectra X LED system. Images were taken using a CFI plan Apochromat Lambda DM 60X oil immersion objective (NA 1.40 WD 0.13MM). During experiments, the microfluidic device was taped to a customized device holder inserted onto the motorized stage (with encoders). In all experiments, the microscope was programmed to acquire images for each channel every 15 min for a total of 80 hours. The exposure and intensity setting for each channel were set as follows: Phase 50 ms, GFP 10 ms at 10% lamp intensity with an EM Gain of 50, mCherry 50 ms at 10% lamp intensity with an EM Gain of 200, and iRFP 300 ms at 15% lamp intensity with an EM Gain of 300. The EM Gain settings are within the linear range.

Quantification of single-cell traces

Fluorescence images were processed with a custom MATLAB code. Background of images from each channel was subtracted. Cell nuclei were identified by thresholding the iRFP images. Each image was evenly divided into 6 parts, each containing a single cell trap. The position of the dent in the cell trap was labeled. In each trap, the positions of all nuclei of each single cell were labeled. Mother cells are identified by comparing the positions of the dent and the positions of nuclei. Since the fluorescence reporter of rDNA silencing is evenly distributed inside the cell, nuclei of mother cells were further dilated to generate a mask to quantify the intensities of fluorescence reporters. The mean intensity value of the top 50% pixels of fluorescence reporter is used as the intensity of the rDNA silencing reporter. All single-cell time traces were normalized by the mean reporter intensity of WT cells' 1^{st} cell cycle and smoothed with local regression using weighted linear least squares and a 2^{nd} degree polynomial model. The normalized and smoothed data were used for plotting of trajectories and density maps.

We also tested segmenting the whole cell using phase images and quantified the mean fluorescence intensities of the whole cell. The resulting time traces were similar to those obtained using nuclei segmentation and quantification as described above. Because nuclei segmentation and quantification is more robust than whole cell segmentation and allows us to identify and analyze more cells automatically, we used the former method for all imaging analysis.

Cell divisions of each mother cell were manually identified and counted at the time that the nuclei separated between mother and daughter cells. Cells were categorized based on their aging phenotypes, characterized by the morphologies of later daughters they produced. Mothers continually producing elongated daughters at the last few generations were categorized as "cells

aging with elongated daughters", whereas mothers continually producing round daughters at the last few generations were categorized as "cells aging with rounded daughters." A small fraction of cells show abnormal morphologies even at the very beginning of the experiment and have a lifespan shorter than 5 generations. Those cells were excluded from analysis.

Development of the phenomenological model of cell aging

A phenomenological model was developed that relates silencing and cell aging based on our experimental data. The model postulates that each mother cell can be in one of two states during aging: state 0 – the silenced state in which it produces normal daughters, and state 1 – the silencing loss state with elongated daughters.

The transitions between the states are purely stochastic and are characterized by transition probabilities p_{01} and p_{10} that depend on the replicative age of the cell. To obtain the transition probabilities from the single-cell data, we computed the fraction of all the cells at the silenced state with normal daughters (state 0) of a given generation that switch to the silencing loss state with elongated daughters (state 1) at the next cell cycle (p_{01}) and the fraction of the cells at the silencing loss state with elongated daughters that return to the silenced state at the next cell cycle (p_{10}), as a function of the replicative age. As the data show, the transition rate from the silenced state to the silencing loss state gradually increases with age, while the rate of the reverse process decreases and reaches zero after ~25 generations (Fig. 4b). Using linear regression, we get $p_{01}(n) = 0.0175 \cdot \text{n-}0.01$ and $p_{10}(n) = 0.28 - 0.0075 \cdot \text{n}$ (n: replicative age).

We also assume that in the silencing loss state (state 1), a damage factor D accumulates over generations. To obtain the relationship between damage accumulation and cell death, we computed the distribution of cell division numbers within the Sustained Phase before cell death and found that it is well approximated by the Poisson distribution with a mean value of 6.7 (Fig. 4c). Based on these data, we assume that the probability of cell death increases with D according to a Poisson cumulative distribution function $F(D,6.7)$. Upon transition back to the silenced state (state 0), D is reset to zero. Finally, based on the experimental data we set the cell cycle length in the silenced state 80 min, and in the silencing loss state, 110 min.

We simulated this model stochastically and generated 100 cell trajectories, ordered based on the replicative life span (Fig. 4d). To simulate the effects of silencing perturbations, we increased p_{01} and decreased p_{10} ten-fold to generate an induced silencing loss (Fig. 4e).

Method References

32 Kitada, K., Yamaguchi, E. & Arisawa, M. Cloning of the Candida glabrata TRP1 and HIS3 genes, and construction of their disruptant strains by sequential integrative transformation. *Gene* **165**, 203-206 (1995).

33 Huang, J. & Moazed, D. Association of the RENT complex with nontranscribed and coding regions of rDNA and a regional requirement for the replication fork block protein Fob1 in rDNA silencing. *Genes & development* **17**, 2162-2176 (2003).

34 Gietz, R. D. & Schiestl, R. H. Quick and easy yeast transformation using the LiAc/SS carrier DNA/PEG method. *Nat Protoc* **2**, 35-37 (2007).

35 Ferry, M. S., Razinkov, I. A. & Hasty, J. Microfluidics for synthetic biology: from design to execution. *Methods Enzymol* **497**, 295-372 (2011).

Figure 1. **Tracking the dynamics of chromatin silencing in single aging cells using a new microfluidic device. a,** The design layout of the device. "Media" points to media inlets; "Cell trapping area" contains cell traps for single mother cells. **b,** A schematic of multiple, parallel cell traps. Mother cells stay at the bottom of finger-shaped chambers while daughters are pushed out. Details of the device are provided in Methods. **c,** Illustrative schematic of the reporter for chromatin silencing. A GFP reporter under a strong constitutive promoter (*TDH3*) is inserted at an NTS1 repeat within the rDNA. Chromatin silencing at the rDNA is reflected by fluorescence intensity: low – silenced, high – decreased silencing. Details of the reporter are provided in Methods. **d,** Time-lapse images of a single cell trap throughout an entire lifespan. Arrows point to the mother cell.

Figure 2. **Dynamic patterns of silencing loss during aging. a,** Dynamics of silencing loss in cells aging with elongated daughters. Top: representative images of cell aging and death with elongated daughters. Arrows point to the mother cell. Bottom: single-cell density map trajectories of reporter fluorescence. Each row represents the time trace of a single cell throughout its lifespan. Color represents the normalized fluorescence intensity as indicated in the color bar, which is used throughout to allow direct comparisons between different conditions. Cells are sorted based on their replicative lifespans (RLS). **b,** Dynamics of silencing loss in cells aging with rounded daughters. **c**, Daughter cell morphology is correlated with the silencing state of mother cells. Density map trajectories of representative mothers are aligned with the morphology (round vs elongated) of daughters produced throughout their lifespans. A cross-correlation analysis of daughter morphology and mother silencing dynamics is shown in Supplementary Fig. 2.

Figure 3. **A quantitative analysis of silencing loss dynamics in single cells. a,** Dynamics of silencing loss in representative single cells with different lifespans. For each cell, (top) time-lapse images for the cell have been shown with (bottom) the fluorescence time trace throughout its lifespan. Vertical dashed line represents each division time of the cell, in which the distance between two adjacent dashed lines indicates the cell cycle length. Reporter fluorescence is normalized to the baseline level (see Methods for details). **b,** A schematic illustrates the dissection of two phases based on the silencing loss dynamics. The rise times of early sporadic and final sustained silencing loss are defined as "t1" and "t2", respectively. **c,** Scatter plots showing the relationships between the length of (left) Intermittent Phase or (right) Sustained Phase and lifespan at the single-cell level. Single-cell data are from Fig. 2a. Each circle represents a single cell. Correlation coefficient (R) is calculated and shown. **d,** Bar graph showing the average durations of (blue) early sporadic and (red) final sustained silencing loss.

Figure 4. A phenomenological model of cell aging. a, Schematic diagram of the two-state stochastic model of cell silencing and aging. **b,** The statistics of silencing state transitions as a function of generations. The fraction of all the cells at the silenced state (state 0) of a given generation that switch to the silencing loss state (state 1) at the next cell cycle (red) and the fraction of the cells at the silencing loss state that return to the silenced state at the next cell cycle

(blue) have been computed as a function of the replicative age. Symbols represent experimental data and lines are linear regressions. **c,** The distribution of cell division numbers within the Sustained Phase before cell death. It is well approximated by the Poisson distribution with a mean value of 6.7. Bar plot – data, red line – fitting by the Poisson distribution. **d,** Single-cell state trajectories from stochastic simulations of the model. Each row represents the time trace of the state of a single cell throughout its lifespan. Blue represents the silenced state (state 0), and red represents the silencing loss state (state 1). Cells are sorted based on their RLSs. **e,** Simulated single-cell trajectories in response to (left) sustained and (right) transient (240 min) silencing loss. Details of the model are included in Methods.

Figure 5. **Perturbations of silencing dynamics shorten lifespan. a,** Dynamics of silencing loss in *sir2*Δ cells. Left: single-cell density map trajectories of reporter fluorescence. Each row represents the time trace of a single cell throughout its lifespan. Color bar is identical to Fig.2. Cells are sorted based on their RLS. The red dashed line represents the average length of Sustained Phase in WT cells, defined in Fig. 3b. Right: representative single-cell time traces with different lifespans. Dynamics of silencing loss in WT cells are shown in response to chemical perturbations: **b,** A 1000-min 5 mM NAM pulse. Inset shows the expression of *RNR3*-mCherry in response to a 1000-min 5 mM NAM pulse at indicated times; **c,** A 240-min 5 mM NAM pulse. Inset shows the expression of *RNR3*-mCherry in response to a 240-min 5 mM NAM pulse at indicated times. **d,** A constant 2.5 mM NA. For each condition, (top) a schematic illustrating the time-based drug treatment has been shown with (bottom) the corresponding single-cell density map trajectories of reporter fluorescence.

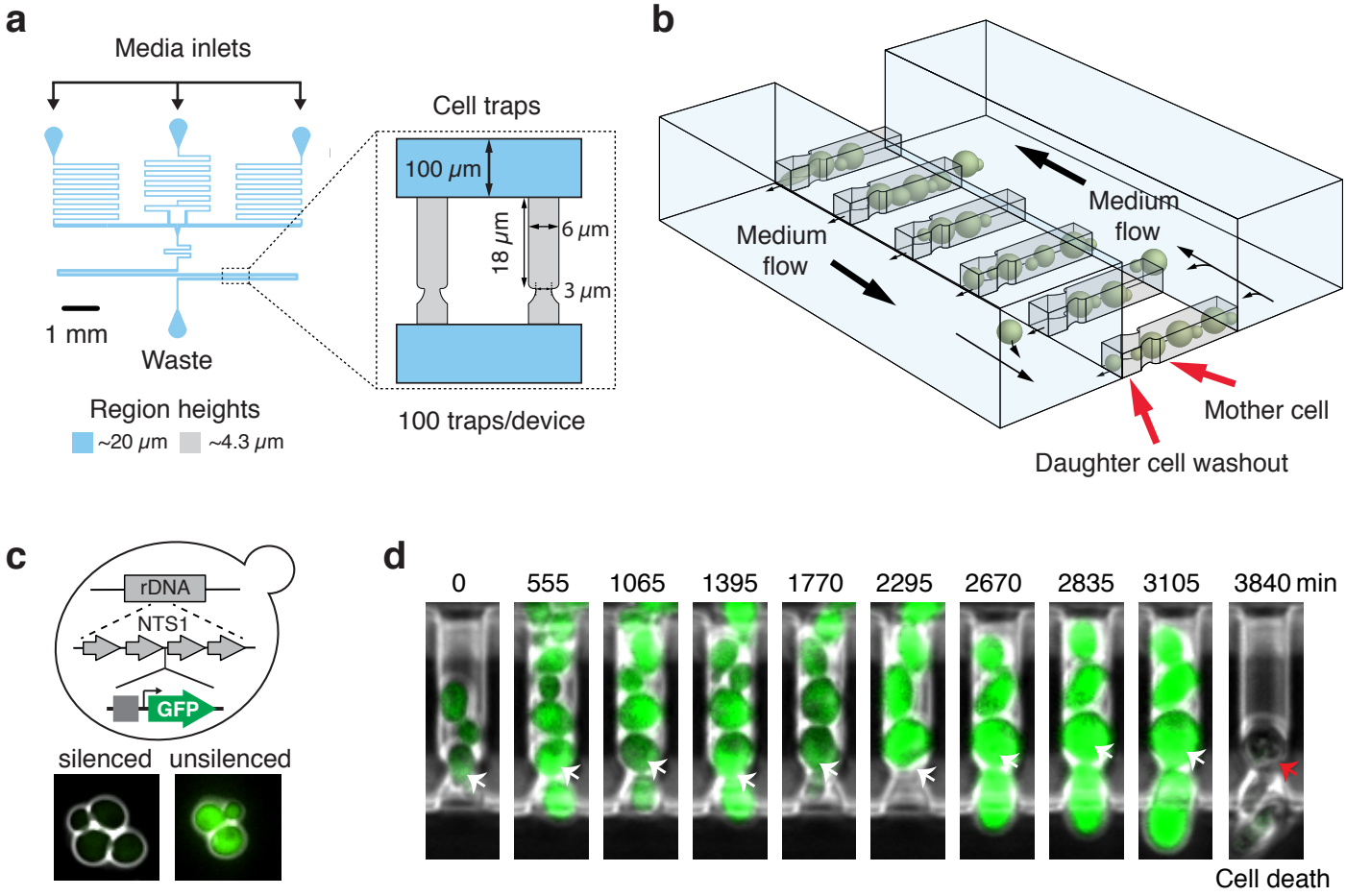

Figure 1. Tracking the dynamics of chromatin silencing in single aging cells using a new microfluidic device. **a,** The design layout of the device. "Media" points to media inlets; "Cell trapping area" contains cell traps for single mother cells. **b,** A schematic of multiple, parallel cell traps. Mother cells stay at the bottom of finger-shaped chambers while daughters are pushed out. Details of the device are provided in Methods. **c,** Illustrative schematic of the reporter for chromatin silencing. A GFP reporter under a strong constitutive promoter (*TDH3*) is inserted at an NTS1 repeat within the rDNA. Chromatin silencing at the rDNA is reflected by fluorescence intensity: low – silenced, high – decreased silencing. Details of the reporter are provided in Methods. **d,** Time-lapse images of a single cell trap throughout an entire lifespan. Arrows point to the mother cell.

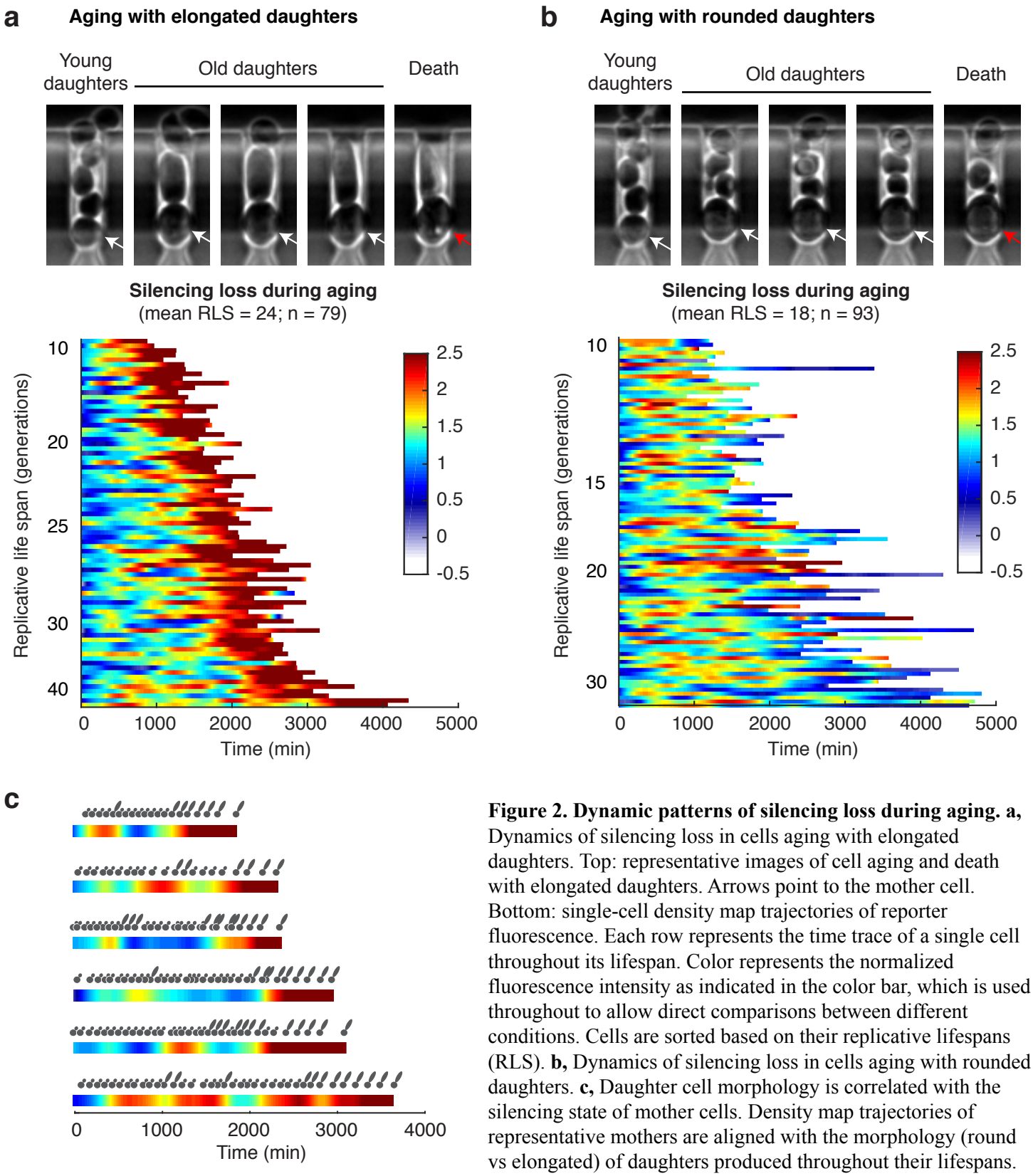

Figure 2. Dynamic patterns of silencing loss during aging. a, Dynamics of silencing loss in cells aging with elongated daughters. Top: representative images of cell aging and death with elongated daughters. Arrows point to the mother cell. Bottom: single-cell density map trajectories of reporter fluorescence. Each row represents the time trace of a single cell throughout its lifespan. Color represents the normalized fluorescence intensity as indicated in the color bar, which is used throughout to allow direct comparisons between different conditions. Cells are sorted based on their replicative lifespans (RLS). **b,** Dynamics of silencing loss in cells aging with rounded daughters. **c,** Daughter cell morphology is correlated with the silencing state of mother cells. Density map trajectories of representative mothers are aligned with the morphology (round vs elongated) of daughters produced throughout their lifespans. A cross-correlation analysis of daughter morphology and mother silencing dynamics is shown in Supplementary Fig. 2.

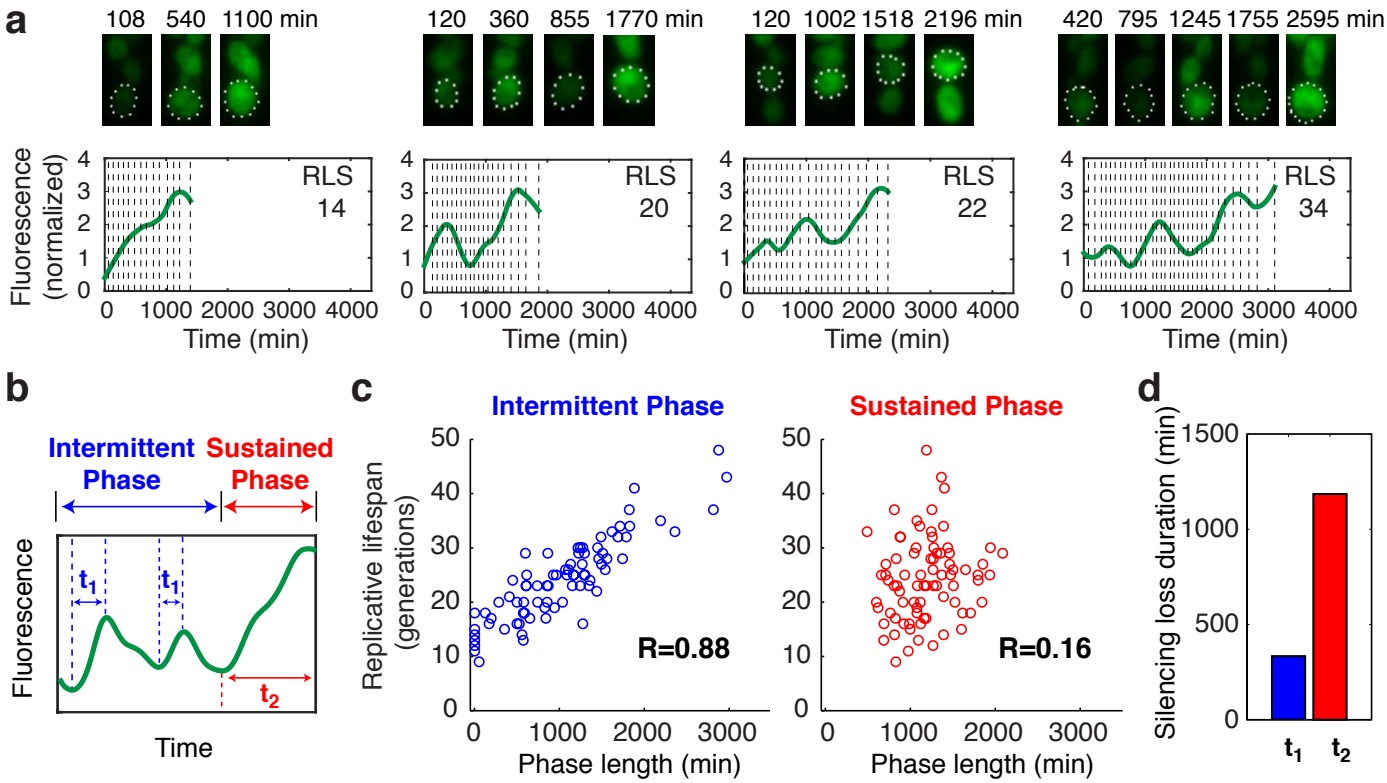

Figure 3. A quantitative analysis of silencing loss dynamics in single cells. a, Dynamics of silencing loss in representative single cells with different lifespans. For each cell, (top) time-lapse images for the cell have been shown with (bottom) the fluorescence time trace throughout its lifespan. Vertical dashed line represents each division time of the cell, in which the distance between two adjacent dashed lines indicates the cell cycle length. Reporter fluorescence is normalized to the baseline level (see Methods for details). **b,** A schematic illustrates the dissection of two phases based on the silencing loss dynamics. The rise times of early sporadic and final sustained silencing loss are defined as "t1" and "t2", respectively. **c,** Scatter plots showing the relationships between the length of (left) Intermittent Phase or (right) Sustained Phase and lifespan at the single-cell level. Single-cell data are from Fig. 2a. Each circle represents a single cell. Correlation coefficient (R) is calculated and shown. **d,** Bar graph showing the average durations of (blue) early sporadic and (red) final sustained silencing loss.

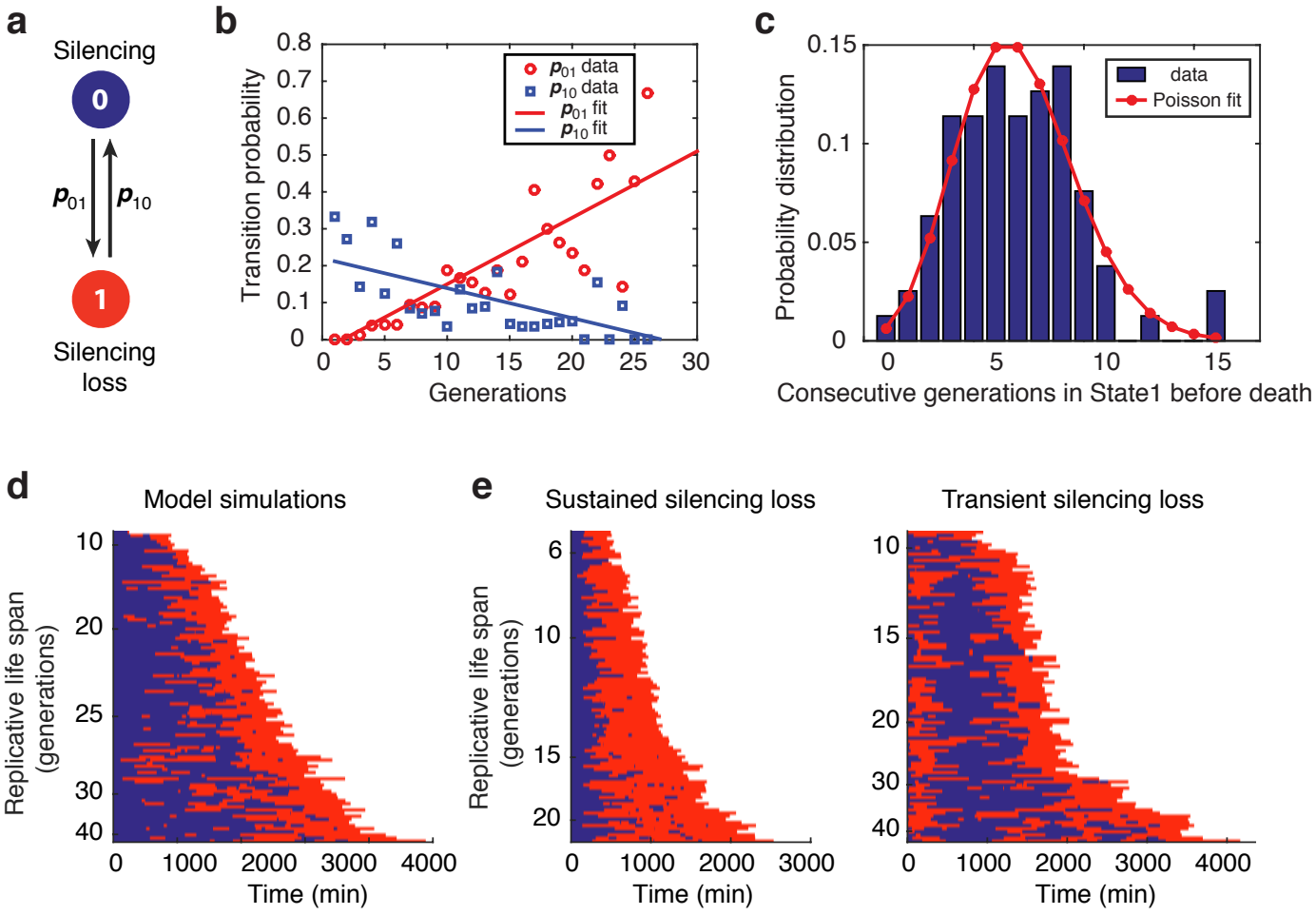

Figure 4. A phenomenological model of cell aging. a, Schematic diagram of the two-state stochastic model of cell silencing and aging. **b,** The statistics of silencing state transitions as a function of generations. The fraction of all the cells at the silenced state (state 0) of a given generation that switch to the silencing loss state (state 1) at the next cell cycle (red) and the fraction of the cells at the silencing loss state that return to the silenced state at the next cell cycle (blue) have been computed as a function of the replicative age. Symbols represent experimental data and lines are linear regressions. **c,** The distribution of cell division numbers within the Sustained Phase before cell death. It is well approximated by the Poisson distribution with a mean value of 6.7. Bar plot – data, red line – fitting by the Poisson distribution. **d,** Single-cell state trajectories from stochastic simulations of the model. Each row represents the time trace of the state of a single cell throughout its lifespan. Blue represents the silenced state (state 0), and red represents the silencing loss state (state 1). Cells are sorted based on their RLSs. **e,** Simulated single-cell trajectories in response to (left) sustained and (right) transient (240 min) silencing loss. Details of the model are included in Methods.

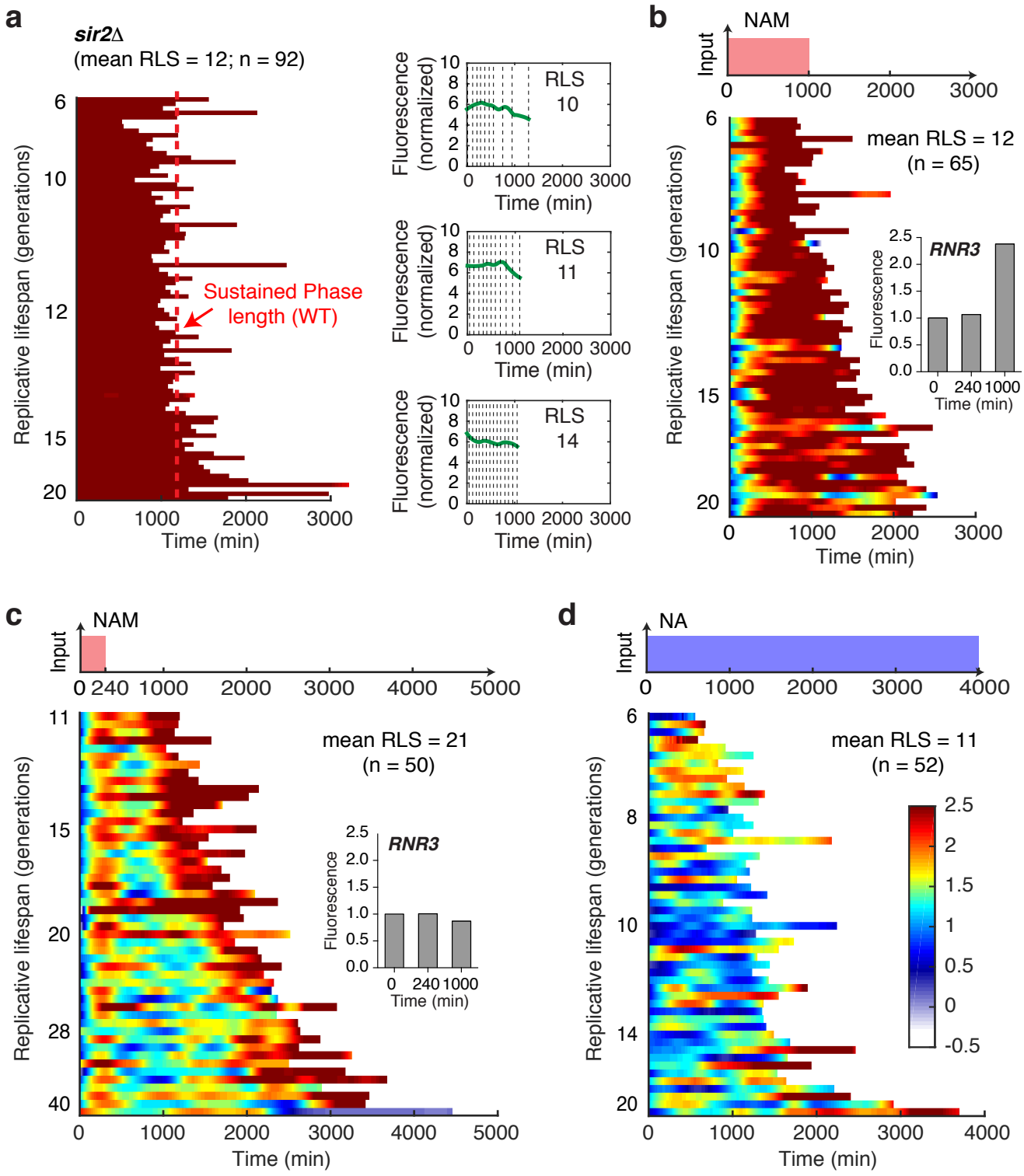

Figure 5. Perturbations of silencing dynamics shorten lifespan. a, Dynamics of silencing loss in *sir2*Δ cells. Left: single-cell density map trajectories of reporter fluorescence. Each row represents the time trace of a single cell throughout its lifespan. Color bar is identical to Fig.2. Cells are sorted based on their RLS. The red dashed line represents the average length of Sustained Phase in WT cells, defined in Fig. 3b. Right: representative single-cell time traces with different lifespans. Dynamics of silencing loss in WT cells are shown in response to chemical perturbations: **b**, A 1000-min 5 mM NAM pulse. Inset shows the expression of *RNR3*-mCherry in response to a 1000-min 5 mM NAM pulse at indicated times; **c,** A 240-min 5 mM NAM pulse. Inset shows the expression of R*NR3*-mCherry in response to a 240-min 5 mM NAM pulse at indicated times; **d,** A constant 2.5 mM NA. For each condition, (top) a schematic illustrating the time-based drug treatment has been shown with (bottom) the corresponding single-cell density map trajectories of reporter fluorescence.

Fig. 5